



## Preparation of poly(acrylonitrile-methacrylate) membrane via thermally induced phase separation: effects of MA with different feeding molar ratios

Na Han\*, Sumei Chen, Guo Chen, Xuefeng Gao, Xingxiang Zhang\*

State Key Laboratory of Hollow Fiber Membrane Materials and Processes, School of Material Science and Engineering, Tianjin Polytechnic University, Tianjin 300387, P.R. China, Tel. +86 22 83955786; emails: [hannapolyu@163.com](mailto:hannapolyu@163.com) (N. Han), [1055231196@qq.com](mailto:1055231196@qq.com) (S. Chen), [616250494@qq.com](mailto:616250494@qq.com) (G. Chen), [gaoxuefeng1992@sina.com](mailto:gaoxuefeng1992@sina.com) (X. Gao), [zhangpolyu@aliyun.com](mailto:zhangpolyu@aliyun.com) (X. Zhang)

Received 20 September 2015; Accepted 2 April 2016

### ABSTRACT

We report the preparation and performance of poly(acrylonitrile-methacrylate) (AN-MA) flat-sheet membranes with various MA feeding ratio via thermally induced phase separation, in which the membrane forming system consisted of AN-MA, ethylene carbonate (EC), and triethyl citrate (TEC). The effects of the preparation conditions, such as the MA feeding mole ratio, EC content in the mixed diluent, and AN-MA concentration on the pore structure, porosity, water flux, and mechanical properties of the AN-MA membranes were studied. The poly(acrylonitrile-methacrylate) (AN-MA mole ratio 85/15, 80/20, 75/25) copolymers were synthesized by emulsion polymerization. The AN-MA copolymers are melt processable in the temperature range of 130–180°C. The morphology of the resulting membrane gradually changes from a typical bicontinuous structure to a cellular structure upon increasing the polymer concentration and EC content in the mixed diluent. The water flux of AN-MA microporous membranes increased and subsequently declined as the MA feeding molar ratio increased in the polymerization system. In addition, the mechanical properties of the AN-MA membranes increased gradually. Consequently, the properties of the AN-MA membranes were optimal when the MA feeding molar ratio was 20 mol%. Correspondingly, the membrane exhibits a relatively high water flux (66.0 L/(m<sup>2</sup> h)) and porosity (75%) when the ternary system contains 60 wt.% EC in the mixed diluent and 9 wt.% 80/20AN-MA. In addition, the membrane exhibits a higher tensile strength (4.6 MPa) and elongation (43.8%).

*Keywords:* Poly(acrylonitrile-methacrylate) membrane; Thermally induced phase separation; MA mole ratio; Morphology; Mechanical property

### 1. Introduction

Microporous membranes can be prepared by many approaches, such as thermally induced phase separation (TIPS) and nonsolvent-induced phase separation

(NIPS), with different mechanisms and membrane structures. NIPS technology requires large amounts of polar, toxic or corrosive solvents, e.g. dimethyl formamide (DMF) or dimethyl sulfoxide (DMSO), which increases the cost and pollutes the air. As an alternative to NIPS, TIPS technology for membrane manufacture has caused extensive attention around

\*Corresponding authors.

world [1–5]. Generally, in the TIPS approach, a homogeneous solution is prepared at an elevated temperature by blending the polymer with the diluent; then, the solution is cooled to induce solid–liquid (S–L) or liquid–liquid (L–L) phase separation, and finally, a microporous structure is formed after the extraction of the diluent [6]. The TIPS method is a promising technology for preparing a porous membrane with advantages including: (1) the absence of macrovoids, (2) better mechanical properties, (3) a narrow pore size distribution, and (4) the possibility of obtaining symmetrical structures [7–10]. The TIPS process has been applied to numerous polymers, such as poly(vinylidene fluoride) (PVDF) [1], polyacrylonitrile (PAN) [2], polyethylene (PE) [3], and polypropylene (PP) [4,5]. Although the preparation of the membranes using this approach is particularly favorable because of fewer control parameters than those in the NIPS process, the wide use of the TIPS process may be limited by the selection of diluent and the high process temperature. The characteristics of the diluents significantly affect the membrane morphology [11–14]. A suitable diluent for membrane preparation via TIPS at high temperature should exhibit miscibility with the polymer, low volatility and good thermal stability.

In TIPS, by varying the composition and temperature, the polymer solutions can be brought into three different regions (a region of spinodal decomposition and two regions of nucleation and growth located between the binodal curve and spinodal curve). When the binodal line, which is the border between the homogeneous solution and phase-separated solution, is located above the crystallization temperature, liquid–liquid (L–L) phase separation occurs [15]. The binodal curve and spinodal curve coincide at the critical point. These three different regions represent the three different mass transport mechanisms that can occur during the membrane formation by liquid–liquid phase separation: (i) nucleation and growth of droplets of the polymer-rich phase followed by solidification of the polymer-rich phase, which forms a bead-like membrane structure; (ii) spinodal decomposition into two interconnected phases with subsequent solidification of the polymer-rich phase, which forms a bicontinuous membrane structure; and (iii) nucleation and growth of droplets of the polymer-lean phase followed by solidification of the polymer-rich phase leading to the formation of a cellular structure [1].

PAN membranes have been widely used in ultrafiltration [16–18], hemodialysis [19], enzyme immobilization [20], and pervaporation [21–23] because PAN exhibits significant characteristics including low cost,

high mechanical properties, good solvent stability, good chemical stability, and excellent biocompatibility. However, only a few studies have been reported on the preparation of PAN membranes via the TIPS method. Xu et al. manufactured PAN membranes with sheet-, needle-, and cellular-like pores via TIPS process using dimethyl sulfoxide (DMSO) and glycerol as the diluent and the non-solvent additive, respectively [24]. They also investigated the effects of DMSO on the pore structure of polar polymer in the TIPS process, including poly(vinylidene fluoride) (PVDF), PAN, and celluloseacetate (CA). The results showed that tubular-like pores are obtained in the PVDF and PAN membranes when crystallizable diluent DMSO was adopted [25]. Based on previous researches, in 2013, they prepared PAN membranes via TIPS process using polyethylene glycol (PEG,  $M_w$ , 200–1,000) as a polymeric additive, which exhibited lacy pores to cellular-like pores with high water flux [26].

However, a macromolecular main chain of PAN exhibits spiraling three-dimensional conformation. There is a stronger dipole force between cyano groups; thus, the PAN membrane exhibits a higher fragility. PAN undergoes a degradation reaction at  $\sim 250^\circ\text{C}$  before melting at  $\sim 320^\circ\text{C}$  [27]. The melt state of PAN is not easy to reach in practice because cyclization and degradation reactions occur below the theoretical melting point [28]. The addition of a flexible second monomer methacrylate to the polymerization system will weaken the strong dipole force and reduce the symmetrical distribution of the polyacrylonitrile macromolecular chain, thereby increasing the flexibility, reducing the melting point, elevating the thermal stability, and mechanical properties of PAN [29].

The primary purpose of this work is to investigate the effects of the AN-MA feeding molar ratios on the pore structure and properties of the membrane prepared via TIPS. Poly(acrylonitrile-methacrylate) copolymers with various feeding molar ratios (85/15, 80/20, 75/25) were synthesized by emulsion polymerization. Moreover, they were melt processable in the temperature range of  $130$ – $180^\circ\text{C}$ . Inspired by the work of Xu [24–26], a crystallizable diluent ethylene carbonate (EC) and a eco-friendly diluent triethyl citrate (TEC) were adopted as mixed diluent in this study. We also investigated the effects of the EC content, polymer concentration, and cooling rates on the pore shape, porosity, water flux and mechanical properties of the AN-MA membranes. The microporous AN-MA membranes prepared via TIPS exhibit controllable structures with high porosity and excellent mechanical properties, which will stabilize the service applications of the membranes in water treatments.

## 2. Experimental section

### 2.1. Materials

Melt-processable AN-MA copolymers were prepared based on our previous work in our laboratory, which were reported in Refs. [30,31]. Relevant physical properties of the AN-MA copolymers are as follows: 85/15AN-MA (the abbreviation 85/15 for the copolymers refers to the feed molar ratio of AN-MA):  $M_n = 26,557$  g/mol,  $M_w = 151,285$  g/mol, melting temperature ( $T_m$ ) = 150–180°C, decomposition temperature ( $T_d$ )  $\approx$  300°C; 80/20AN-MA:  $M_n = 42,304$  g/mol,  $M_w = 555,208$  g/mol,  $T_m = 120$ –140°C,  $T_d \approx 315$ °C; 75/25AN-MA:  $M_n = 79,954$  g/mol,  $M_w = 1,177,338$  g/mol,  $T_m = 120$ –140°C,  $T_d \approx 324$ °C. Ethylene carbonate (EC) was obtained from Aladdin Reagent Inc. (China). Triethyl citrate was purchased from Weifang Dimon Chemical Co., Ltd. Deionized water was used as the extractant. The AN-MA copolymers were dried before use, and the other chemicals were used without further purification.

### 2.2. Preparation of AN-MA membranes

The AN-MA/EC/TEC mixture was heated until a homogeneous solution was obtained. After degassing any air bubbles, the solution was preheated in an oven. The resulting solution was cast onto a glass plate using a glass rod with a gap of 0.3 mm, immediately followed by immersion of the polymer dope into a 0°C water bath for phase separation. When the solution was completely solidified, the nascent membrane was removed from the glass plate and immersed in deionized water at room temperature. A wet AN-MA membrane was obtained after the diluents were extracted. The specific compositions and preparation conditions for each AN-MA membrane are listed in Table 1. The samples were denoted as  $xP(yEzT)$ , where P, E, and T represent AN-MA, EC, and TEC, respectively, and  $x$ ,  $y$ , and  $z$  denote the corresponding mass fraction of AN-MA, EC, and TEC, respectively. P1, P2, and P3 represent 85/15AN-MA, 80/20AN-MA, and 75/25AN-MA, respectively.

### 2.3. Scanning electron microscopy (SEM) observation

Field-emission scanning electron microscopy (FESEM, HitachiS-4800, Japan) was employed to investigate the morphologies of the membranes. A dry AN-MA membrane was frozen and fractured in liquid nitrogen to obtain a tidy cross section. After the samples were sputtered with gold using a sputter coater (SCD-005), the cross section and top and bottom

surfaces were imaged by FESEM at an acceleration voltage of 10.0 kV.

### 2.4. Water permeation measurement

The water flux was determined using a homemade device with a pressurized stirred test cell. Each membrane sample of approximately 18 cm<sup>2</sup> was first installed into the permeation cell and compacted by filtering ultrapure water at 0.12 MPa and 25°C for 30 min. Then, the pressure was reduced to the operation pressure, 0.10 MPa. The pure water flux ( $J_w$ ) was measured until consecutive recorded values differed by less than 2%; the value was calculated using the following equation:

$$J_w = V/(A\Delta t) \quad (1)$$

where  $V$ ,  $A$ , and  $\Delta t$  represent the volume of permeated water (L), the membrane area (m<sup>2</sup>), and the permeation time (h), respectively. For each sample, three membranes were measured in parallel, and the average water flux was reported.

### 2.5. Pore size and porosity determination

The average pore size of each AN-MA membrane was determined using the software Image-Pro Plus 6.0 (IPP6.0) [32].

The porosity is defined as the volume of pores divided by the total volume of the membrane [33]. A wet AN-MA membrane was first weighed as soon as the superficial water of the wet membrane was removed with dry filter paper. The wet membrane was dried in a vacuum oven for 48 h at 50°C. After drying, the weight of the dry membrane was measured again. The porosity of the wet AN-MA membrane was denoted as  $\varepsilon$ , which was determined by the gravimetric method:

$$\varepsilon = \frac{(m_1 - m_2)/\rho_{\text{water}}}{(m_1 - m_2)/\rho_{\text{water}} + m_2/\rho_{\text{AN-MA}}} \times 100\% \quad (2)$$

where  $m_1$  is the weight of the wet AN-MA membrane,  $m_2$  is the weight of the dry AN-MA membrane, and  $\rho_{\text{water}}$  and  $\rho_{\text{AN-MA}}$  are the density of water and the AN-MA copolymer, respectively.  $\rho_{\text{AN-MA}}$  was obtained by weighting method. The AN-MA copolymers in powder form were placed in a circle mold formed by stacking multiple layers of iron sheets. The powders in the mold were compressed under a pressure. The average thickness and diameter of the samples were

Table 1  
Preparation conditions of AN-MA membranes

Sample	Component of ternary system	AN-MA concentration (wt.%)	EC content in the mixed diluent (wt.%)	TEC content in the mixed diluent (wt.%)	Cooling bath (°C)	Membrane-forming situation
1	9P1 (60E40T)	9	60	40	0	–
2	9P1 (65E35T)	9	65	35	0	–
3	9P1 (70E30T)	9	70	30	0	–
4	9P1 (75E25T)	9	75	25	0	–
5	12P1 (60E40T)	12	60	40	0	–
6	12P1 (65E35T)	12	65	35	0	–
7	12P1 (70E30T)	12	70	30	0	–
8	12P1 (75E25T)	18	75	25	0	–
9	15P1 (60E40T)	15	60	40	0	–
10	15P1 (65E35T)	15	65	35	0	+
11	15P1 (70E30T)	15	70	30	0	+
12	15P1 (75E25T)	15	75	25	0	+
a	9P2 (60E40T)	9	60	40	0	+
b	9P2 (65E35T)	9	65	35	0	+
c	9P2 (70E30T)	9	70	30	0	+
d	9P2 (75E25T)	9	75	25	0	+
e	12P2 (60E40T)	12	60	40	0	+
f	12P2 (65E35T)	12	65	35	0	+
g	12P2 (70E30T)	12	70	30	0	+
h	12P2 (75E25T)	12	75	25	0	+
i	15P2 (60E40T)	15	60	40	0	+
j	15P2 (65E35T)	15	65	35	0	+
k	15P2 (70E30T)	15	70	30	0	+
l	15P2 (75E25T)	15	75	25	0	+
A	9P3 (60E40T)	9	60	40	0	+
B	9P3 (65E35T)	9	65	35	0	+
C	9P3 (70E30T)	9	70	30	0	+
D	9P3 (75E25T)	9	75	25	0	+
E	12P3 (60E40T)	12	60	40	0	+
F	12P3 (65E35T)	12	65	35	0	+
G	12P3 (70E30T)	12	70	30	0	+
H	12P3 (75E25T)	12	75	25	0	+
I	15P3 (60E40T)	15	60	40	0	+
J	15P3 (65E35T)	15	65	35	0	+
K	15P3 (70E30T)	15	70	30	0	+
L	15P3 (75E25T)	15	75	25	0	+

Notes: –: represents that a membrane cannot form, +: represents that a membrane can be formed.

measured by micrometer and at least three specimens were tested for accuracy.

### 2.6. Tensile tests

The tensile strength and elongation of the AN-MA membranes were evaluated using a tensile test instrument (SANS, MTS SYSTEMS Co., Ltd, China). The test was performed at a strain rate of 20 mm/min at room temperature. The membrane samples were prepared with rectangular shapes with a gage length of 20 mm and a width of 10 mm. The thickness was precisely

measured using a spiral micrometer implement. The tensile strength and elongation data were determined based on the stress–strain curve. Each data point was the average of at least six parallel experiments.

## 3. Results and discussion

### 3.1. Solubility parameters for AN-MA/EC/TEC ternary system

The miscibility of the ternary system studied here primarily depends on the solubility parameter  $\delta$ .

Table 2  
Solubility parameters for AN-MA and mixed diluent

Material	$V_m$ (cm <sup>3</sup> /mol)	$\delta_d$ (MPa <sup>0.5</sup> )	$\delta_p$ (MPa <sup>0.5</sup> )	$\delta_h$ (MPa <sup>0.5</sup> )	$\delta$ (MPa <sup>0.5</sup> )
85/15AN-MA	286.07	19.60	9.67	8.20	23.34
80/20AN-MA	219.6	19.49	10.77	8.26	23.75
75/25AN-MA	180.5	19.39	11.60	8.32	24.08
EC	66.62	15.46	14.34	10.96	23.76
TEC	234.73	16.70	6.75	12.21	21.76
60E40T	–	16.00	11.08	11.52	22.61
65E35T	–	15.93	11.48	11.45	22.73
70E30T	–	15.86	11.87	11.38	22.85
75E25T	–	15.80	12.27	11.31	22.98
80E20T	–	15.73	12.68	11.24	23.12

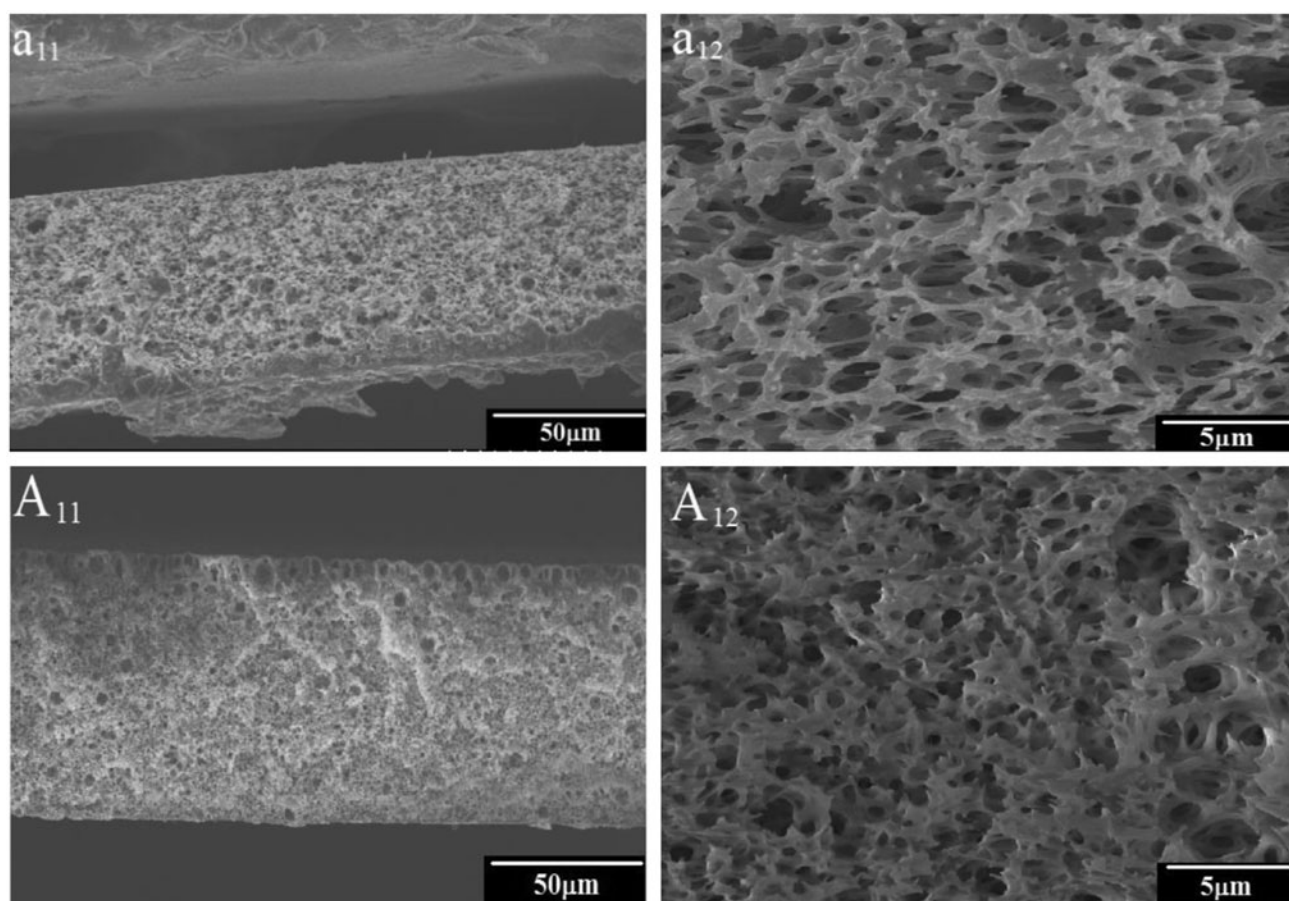


Fig. 1. SEM images of AN-MA membranes prepared from 9 wt.% AN-MA: (a<sub>11</sub>, a<sub>12</sub>) P2 and (A<sub>11</sub>, A<sub>12</sub>) P3. The membranes were prepared from the ternary system with 60 wt.% EC content in the mixed diluent: (a<sub>11</sub>, A<sub>11</sub>) 600× and (a<sub>12</sub>, A<sub>12</sub>) 5,000×.

The overall and individual solubility parameters of AN-MA, EC, TEC, and the mixed diluent are listed in Table 2. The overall solubility parameter ( $\delta$ ) is given by the sum of the dispersion ( $\delta_d$ ), polar ( $\delta_p$ ), and hydrogen bonding ( $\delta_h$ ) contributions, which represents the strength of physical bonding of a material. The

solubility parameters of AN-MA, EC, TEC, and the mixed diluent (Table 2) were calculated using the group molar attraction constants given by van Krevelen and Te Nijenhuis [34]. The  $V_m$  of AN-MA was calculated according to idea expressed by Coleman [35]. The  $V_m$  of the diluent is the molecular

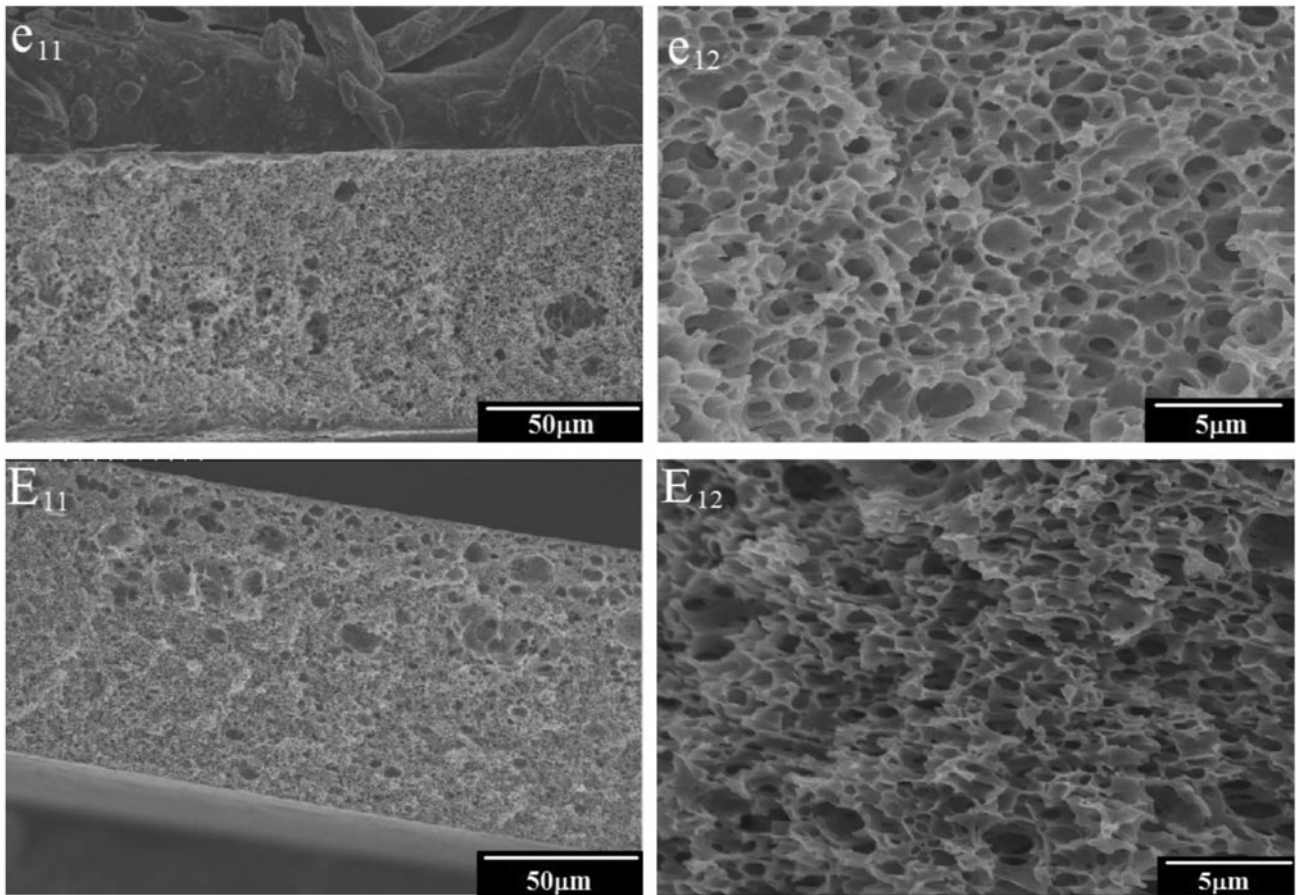


Fig. 2. SEM images of AN-MA membranes prepared from 12 wt.% AN-MA: ( $e_{11}$ ,  $e_{12}$ ) P2 and ( $E_{11}$ ,  $E_{12}$ ) P3. The membranes were prepared from the ternary system with 60 wt.% EC content in the mixed diluent: ( $e_{11}$ ,  $E_{11}$ ) 600 $\times$  and ( $e_{12}$ ,  $E_{12}$ ) 5,000 $\times$ .

weight divided by its density. Hansen's parameters, such as  $\delta_d$ ,  $\delta_p$ ,  $\delta_h$ , and  $\delta$ , can be directly calculated using the following equations:

$$\delta_d = \frac{\sum_i F_{d,i}}{V_m} \quad (3)$$

$$\delta_p = \frac{\sqrt{\sum_i F_{p,i}^2}}{V_m} \quad (4)$$

$$\delta_h = \sqrt{\frac{\sum_i E_{h,i}}{V_m}} \quad (5)$$

$$\delta^2 = \delta_d^2 + \delta_p^2 + \delta_h^2 \quad (6)$$

Here,  $i$  is the number of structural groups,  $F_{d,i}$  and  $F_{p,i}$  are the group molar attractions and  $E_{h,i}$  is the cohesive energy contributed from hydrogen bonding. AN-MA

has an overall solubility parameter closer to 80E20T, which indicates that the polymer-diluent system becomes more compatible as the EC content increases in the mixed diluent. Even the P1/EC/TEC system becomes incompatible when the EC content is lower than 60 wt.% in the mixed diluent. Moreover, the compatibility between AN-MA and the mixed diluent becomes poor with the increase of the MA feeding molar ratio in polymerization, which indicates that the phase separation is not more likely to occur with the increase of the MA content.

### 3.2. Membrane structure

#### 3.2.1. Effects of AN-MA concentration on the membrane structure

Figs. 1–3 show the cross-section morphologies of AN-MA membranes prepared from the ternary system with various AN-MA concentrations. A membrane is

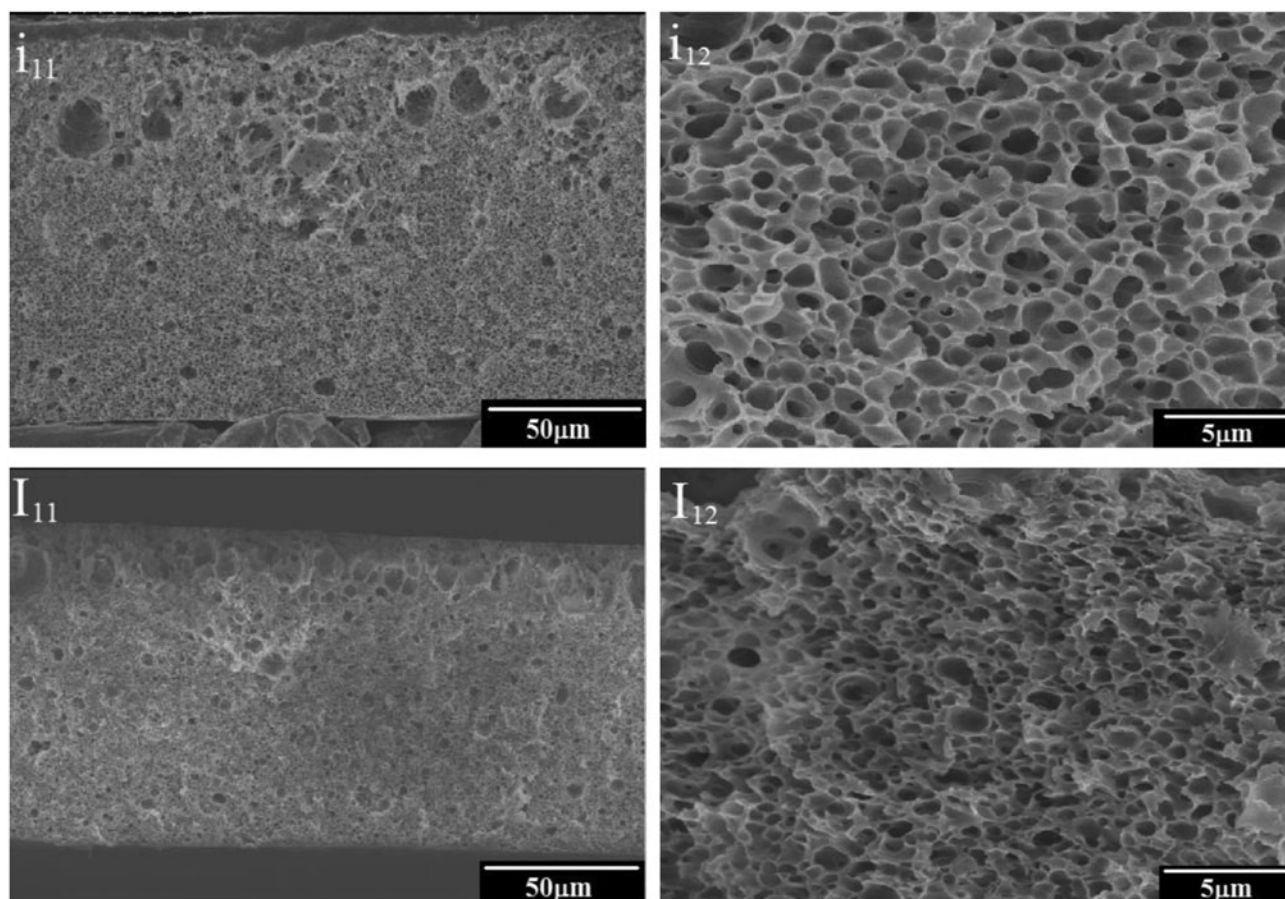


Fig. 3. SEM images of AN-MA membranes prepared from 15 wt.% AN-MA: ( $i_{11}$ ,  $i_{12}$ ) P2 and ( $I_{11}$ ,  $I_{12}$ ) P3. The membranes were prepared from the ternary system with 60 wt.% EC content in the mixed diluent: ( $i_{11}$ ,  $I_{11}$ ) 600 $\times$  and ( $i_{12}$ ,  $I_{12}$ ) 5,000 $\times$ .

unable to form when the P1 concentration is 9 and 12 wt.% because of the lower molecular weight of P1.

The effects of the AN-MA concentration on the structure of the membranes were investigated while maintaining the EC content constant at 60 wt.% and phase separation in a 0 $^{\circ}$ C water bath. Figs. 1–3 show the morphologies of the cross sections of AN-MA membranes with the AN-MA concentration ranging from 9 to 15 wt.%. These scanning electron microscopy (SEM) images reveal that the morphology of the membranes is primarily composed of two types of structures: a bicontinuous and cellular structure. In addition, no obvious spherulites are observed due to the liquid–liquid phase separation before polymer crystallization. The cross-section structure of the AN-MA membranes changes from bicontinuous pores to a cellular-like pore structure with the emergence of closed pores with an increase in the AN-MA concentration from 9 to 15 wt.%. The bicontinuous structure with nearly uniform pore size shown in Fig. 1 is due to spinodal decomposition with

subsequent solidification of the polymer-rich phase for the AN-MA/EC/TEC system. For an explanation of the changes in the morphology at higher polymer concentration, at which AN-MA formed a cellular structure, a mechanism of nucleation and growth of polymer-lean droplets with further solidification of the polymer-rich phase is considered [36]. The AN-MA microporous membranes were obtained by immersion of the solutions in the 0 $^{\circ}$ C water bath. Heat transfer is generally about two orders faster than mass transfer in liquids [37]. Thus, when the polymer solution was immersed in the 0 $^{\circ}$ C water bath, TIPS occurred before NIPS. The solution took shape diluent-rich and diluent-poor phases after going through TIPS. Under the TIPS membrane preparation condition, the diluent-rich phase formed droplets. Over time, the process of the droplets grew through was coarsening. At the end of the coarsening stage, the solution was further cooled to restrain the growth due to the solidifying of diluent-poor phase. Once the crystallization, the solution solidified to establish the nascent morphology of the

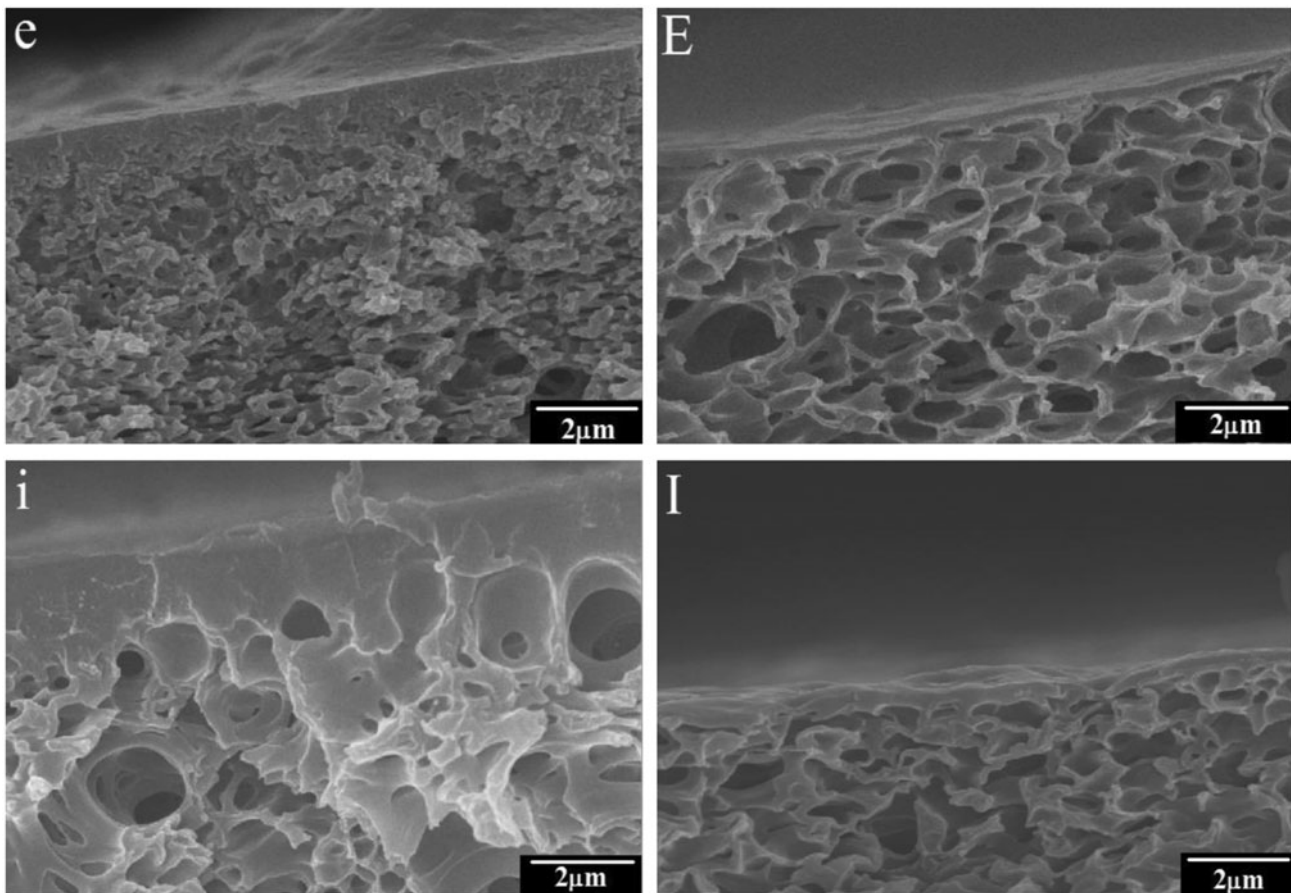


Fig. 4. SEM images of AN-MA membranes prepared from 12 to 15 wt.% AN-MA: (e, E) 12 wt.%, (i, I) 15 wt.%, (e, i) P2, and (E, I) P3. The membranes were prepared from the ternary system with 60 wt.% EC content in the mixed diluent: 10,000 $\times$ .

membrane. Ultimately, the diluent was extracted to form a cellular structure after the solidification of the system [38]. When the AN-MA concentration increases, first, because of the high viscosity of the system with the increase in the AN-MA concentration, the coarsening of the droplets is slower. Second, the polymer-lean phase volume fraction is smaller; thus, there are not enough diluents for the droplets to grow. Therefore, the diluent is extracted to yield isolated cellular pores; the cross sections of the membrane in Figs. 2 and 3 reveal a morphology of weakly connected cellular pores when the AN-MA concentration is 12 and 15 wt.%.

### 3.2.2. Effects of MA feeding ratio on the membrane structure

The cross-section structure of the membranes changes slightly with increasing MA content from 20 to 25 mol% except for the reduction of the skin layer

thickness (Fig. 4). The side chain of the AN-MA copolymer contains polar groups  $-\text{CN}$ , and the polymer rapidly solidified when the polymer contacted water, inducing a dense skin layer on the surface of the AN-MA membrane. The polarity of the AN-MA copolymer weakens upon increasing the MA content, leading to the reduction of the skin layer thickness of the AN-MA membrane after immersion in a 0 $^{\circ}\text{C}$  water bath.

Moreover, the interconnectivity among the pores of the AN-MA microporous membrane decreased with increasing of the MA content (Fig. 1). On the one hand, when the MA feed molar ratio increases from 20 to 25 mol%, the molecular weight of the AN-MA copolymer increases from 555,208 to 1,177,338 g/mol. However, the association between the hydrogen bond and carbonyl group on the polymer molecules was conducive to increase the viscosity of the casting solution when the MA content increased. Therefore, the coarsening process of the system becomes slow when

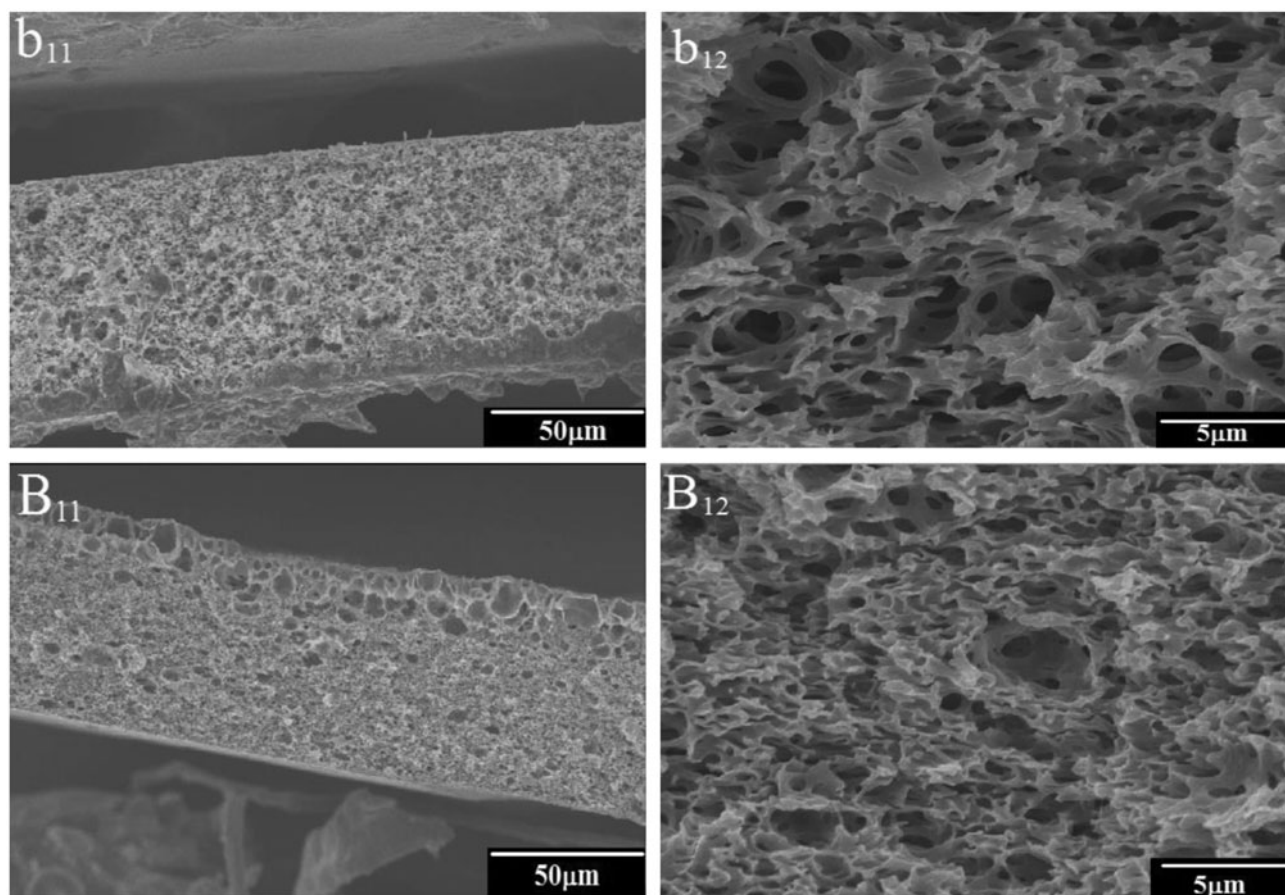


Fig. 5. SEM images of AN-MA membranes prepared from 9 wt.% AN-MA: ( $b_{11}$ ,  $b_{12}$ ) P2 and ( $B_{11}$ ,  $B_{12}$ ) P3. The membranes were prepared from the ternary system with 65 wt.% EC content in the mixed diluent: ( $b_{11}$ ,  $B_{11}$ ) 600 $\times$  and ( $b_{12}$ ,  $B_{12}$ ) 5,000 $\times$ .

the MA mole ratio is as high as 25 mol%. However, there are more continuous phases formed by the polymer-rich phase in the L-L phase separation process in this case. Following the solidification of the matrix phase, most of the diluent was extracted to yield a weakly connected pore structure.

### 3.2.3. Effects of EC content on the membrane structure

Figs. 1 and 5–7 show the cross-section morphologies of AN-MA membranes prepared from the ternary system with various EC contents in the mixed diluent. The structure of the membranes changed from interconnected network-like pores (Figs. 1 and 5) to cellular-like pores (Figs. 6 and 7) when the EC content in the mixed diluent changed from 60 to 75 wt.%. When the polymer solution is cooled down to the liquid–liquid phase separation region, the solution separates into a polymer-rich continuous phase and a polymer-lean droplet phase, or bicontinuous polymer-rich and

polymer-lean phases, depending on the nucleation and growth (NG) mechanism or spinodal decomposition (SD) mechanism [39]. At the cooling condition, we can deduce that the interconnected network-like structure observed in Figs. 1 and 4 is due to spinodal decomposition with subsequent solidification of the polymer-rich phase for the AN-MA/EC/TEC system [10]. Because the homogeneous mixture was quenched from high temperature to the 0 $^{\circ}$ C water bath, the cooling rate is so fast that the phase separation directly entered into the unstable region and proceeded through spinodal decomposition. In addition, the coarsening process was negligible under this condition. An explanation of the changes in the morphology at higher EC content at which P2/P3 formed a cellular structure is considered a mechanism of nucleation and growth of polymer-lean droplets with further solidification of the polymer-rich phase. The increase in the EC content leads to a low cloud point at a given polymer concentration, which is attributed to the

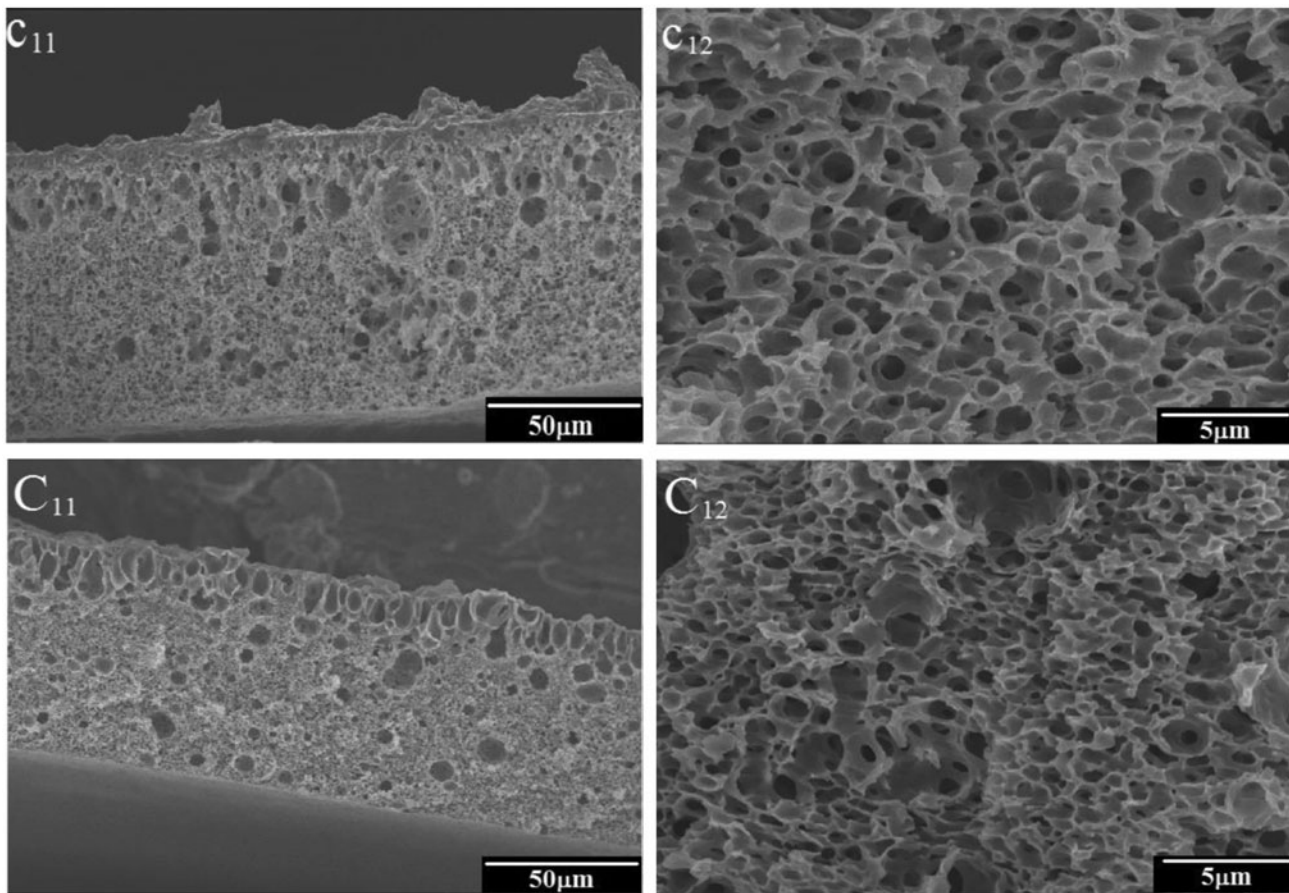


Fig. 6. SEM images of AN-MA membranes prepared from 9 wt.% AN-MA: ( $c_{11}$ ,  $c_{12}$ ) P2 and ( $C_{11}$ ,  $C_{12}$ ) P3. The membranes were prepared from the ternary system with 70 wt.% EC content in the mixed diluent: ( $c_{11}$ ,  $C_{11}$ ) 600 $\times$  and ( $c_{12}$ ,  $C_{12}$ ) 5,000 $\times$ .

compatibility between AN-MA and the mixed diluent improving with the addition of EC. Upon cooling, the system undergoes nucleation and growth of liquid–liquid phase separation before solidification, which leads to the cellular structure.

### 3.3. Pore size and distribution

The pore sizes of the AN-MA membranes obtained by quenching AN-MA/EC/TEC solutions at various AN-MA concentrations and EC contents in the mixed diluent into a 0 $^{\circ}$ C water bath are listed in Table 3. The pore size of the AN-MA membranes decreases with increasing AN-MA concentration and EC content in the mixed diluent. First, by increasing the EC content, there is less time for the coarsening of droplets due to the shorter time interval from the cloud point to the crystallization. Second, because of the high viscosity of the system with increasing AN-MA concentration, coarsening of the droplets is slower. Finally, as the AN-MA concentration increases, the polymer-lean

phase volume fraction is smaller; thus, there are not enough diluents for the droplets to grow. A lower concentration of AN-MA resulted in a longer growth time of the diluent-rich phase and subsequently a larger pore size [40].

In addition, Table 3 also shows that the pore size of the AN-MA membranes increases and then decreases as the MA content increases from 15 to 25 mol%. The polar group –CN content of the AN-MA copolymer is relatively high when the MA content is 15 mol%. The polymer solidifies rapidly upon contacting with water, forming a dense skin layer on the surface of membrane. Then, the dense skin layer restrains liquid–liquid phase separation of the system, and the pore size is relatively small due to the shorter growth time of the polymer-lean phase. The molecular weight of the AN-MA copolymer increases with increasing MA content. The viscosity of the casting solution is so high when the MA content is 25 mol% that the polymer-lean droplets have less time to grow and the growth rate is slower. Therefore, the pore size of

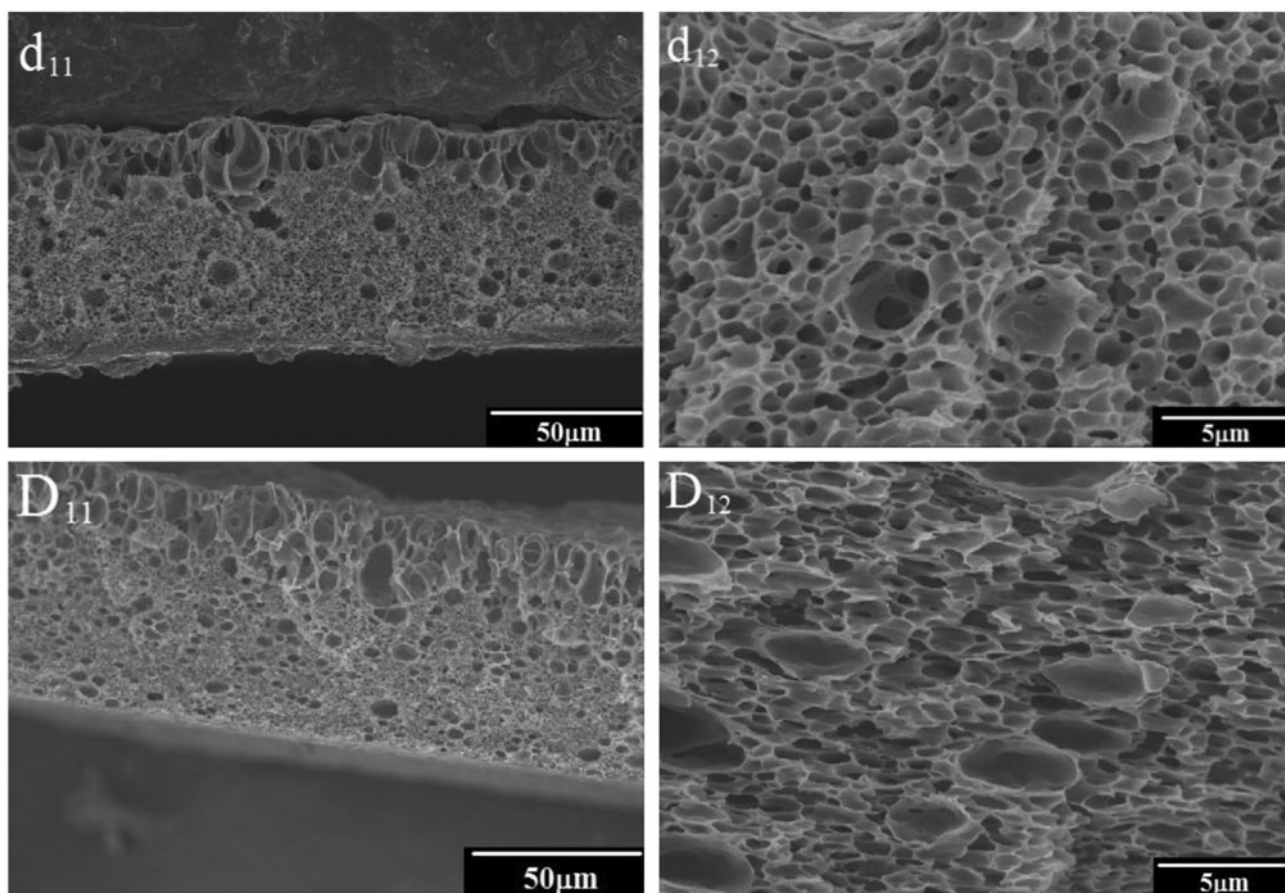


Fig. 7. SEM images of AN-MA membranes prepared from 9 wt.% AN-MA: ( $d_{11}$ ,  $d_{12}$ ) P2 and ( $D_{11}$ ,  $D_{12}$ ) P3. The membranes were prepared from the ternary system with 75 wt.% EC content in the mixed diluent: ( $d_{11}$ ,  $D_{11}$ ) 600 $\times$  and ( $d_{12}$ ,  $D_{12}$ ) 5,000 $\times$ .

the resulting membrane is relatively small. Consequently, the pore size of the AN-MA membranes is the largest when the MA content is 20 mol%.

The pore size distribution curves of the AN-MA membranes prepared from different MA contents at a 15 wt.% polymer concentration are presented in Figs. 8–10. The results indicate that the pore sizes of the resulting membranes exhibit narrow distributions. The pore size distributions are approximately 1.3–1.6  $\mu\text{m}$ , 1.4–1.8  $\mu\text{m}$  and 1.3–1.7  $\mu\text{m}$  for the 15P1 (65E35T), 15P2 (65E35T), and 15P3 (65E35T) systems, respectively. Therefore, it is suggested that the pore sizes of the AN-MA microporous membrane prepared via TIPS are apt to be controlled in a narrow distribution.

### 3.4. Water flux and porosity

#### 3.4.1. Effects of AN-MA concentration and feed ratio of MA on the water flux and porosity of the membrane

We studied the effects of the polymer concentration and MA feed ratio on the water flux and porosity

of AN-MA membranes (Figs. 11 and 12). The results indicate that the water flux and porosity of AN-MA membranes increase with decreasing polymer concentration. This development trend is predictable. The membrane pore structure mainly originates from the space occupied by the diluent. The content of the diluent decreases with the increase in the AN-MA concentration; consequently, the porosity and water flux decrease. Generally, in the TIPS process, the higher polymer concentration results in smaller pores. Because the diluent was introduced in the outer surface of the membrane at high temperature, and the outer surface of the membrane was immersed in a relatively cold water bath, the cooling rate of the outer surface is faster than that of the bottom surface. Furthermore, the polymer concentration near the outer surface is greater than that near the bottom surface because of the evaporation of diluent. Thus, there is a denser skin layer on the surface of the membrane when the AN-MA concentration is relatively high. When the polymer concentration is as low as 9 wt.%,

Table 3  
Average pore size of AN-MA membranes

Ratio of mixed diluent and the type of AN-MA	Pore size ( $\mu\text{m}$ )	AN-MA concentration (wt.%)		
		9P	12P	15P
60E40T	P1	–	–	–
	P2	$2.4 \pm 0.4$	$1.7 \pm 0.3$	$1.6 \pm 0.2$
	P3	$1.9 \pm 0.5$	$1.6 \pm 0.3$	$1.4 \pm 0.4$
65E35T	P1	–	–	$1.4 \pm 0.2$
	P2	$2.2 \pm 0.3$	$1.6 \pm 0.4$	$1.5 \pm 0.4$
	P3	$1.6 \pm 0.5$	$1.5 \pm 0.5$	$1.4 \pm 0.3$
70E30T	P1	–	–	$1.2 \pm 0.3$
	P2	$1.5 \pm 0.4$	$1.4 \pm 0.4$	$1.4 \pm 0.2$
	P3	$1.4 \pm 0.3$	$1.3 \pm 0.4$	$1.2 \pm 0.4$
75E25T	P1	–	–	$1.1 \pm 0.3$
	P2	$1.3 \pm 0.2$	$1.3 \pm 0.1$	$1.2 \pm 0.5$
	P3	$1.2 \pm 0.3$	$1.1 \pm 0.2$	$1.0 \pm 0.3$

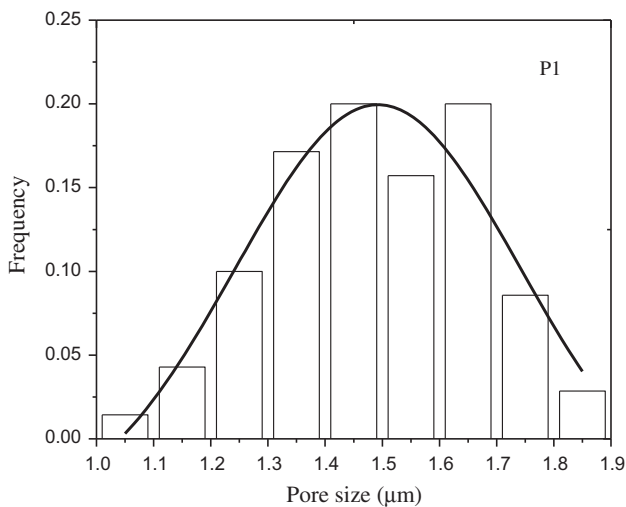


Fig. 8. Pore size distribution curve of AN-MA membranes prepared by 15P1 (65E35T) in water bath at 0°C.

the AN-MA membrane possesses the highest water flux and porosity because of the well-interconnected network-like structure with nearly uniform pore size.

In addition, Fig. 12 reveals that the water flux of AN-MA membranes increases and then decreases as the MA content increases in the system. However, the water flux of the P1 membrane is quite small even though its porosity remains quite high. First, a dense skin layer may account for the low water flux of the P1 membrane. The polar group–CN content of the

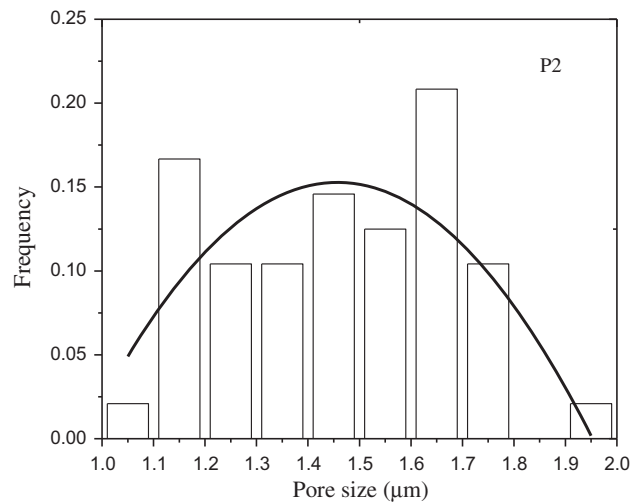


Fig. 9. Pore size distribution curve of AN-MA membranes prepared by 15P2 (65E35T) in water bath at 0°C.

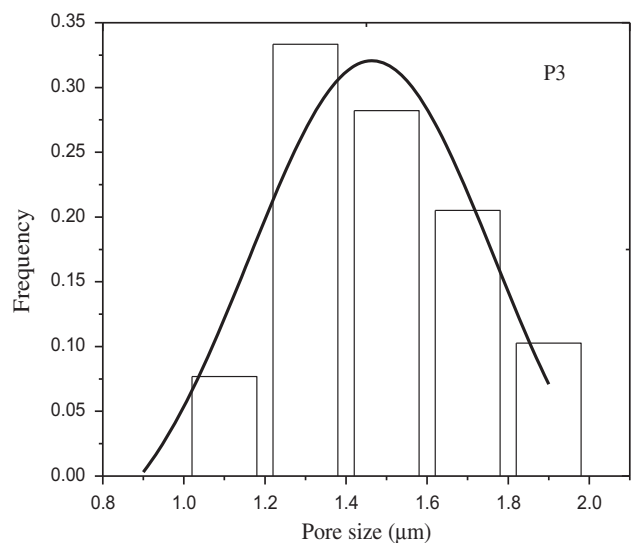


Fig. 10. Pore size distribution curve of AN-MA membranes prepared by 15P3 (65E35T) in water bath at 0°C.

AN-MA copolymer is relatively high when the MA content is 15 mol%. The polymer solidifies rapidly upon contacting water, forming a dense skin layer on the surface of the membrane. Second, the dense skin layer restrains liquid–liquid phase separation of the system, resulting in numerous isolated cellular pores. With increasing MA content, the molecular weight of the AN-MA copolymer increases. The viscosity of the casting solution is so high when the MA content is 25 mol% that the polymer-lean droplets have less time to grow and the growth rate is slower. The pore size of the resulting membrane is relatively small, resulting in a lower porosity and water flux of the P3

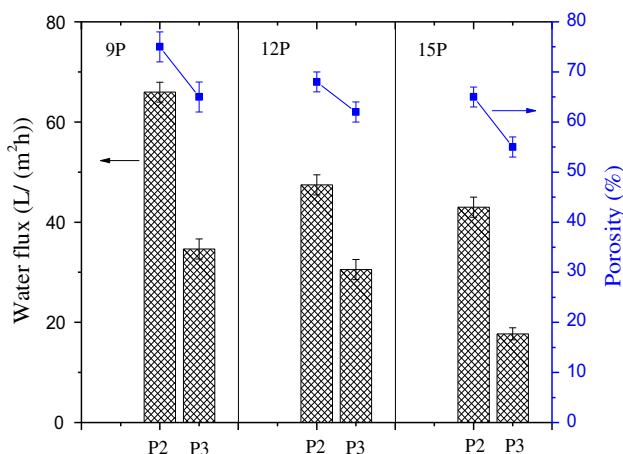


Fig. 11. Water flux and porosity of AN-MA membranes varied with AN-MA concentration and feed ratio of MA. The membranes were prepared from the ternary system with 60 wt.% EC content in the mixed diluent.

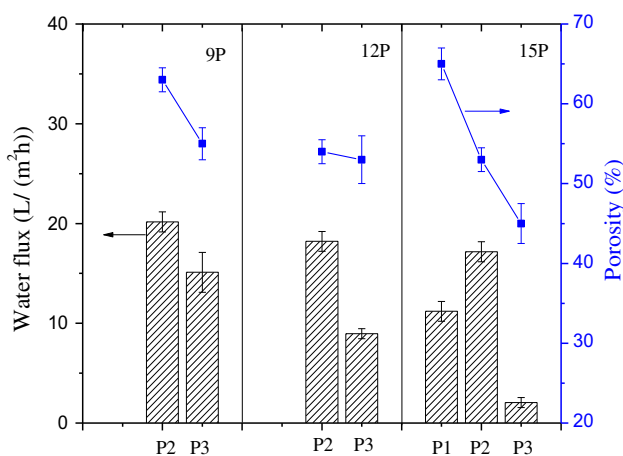


Fig. 12. Water flux and porosity of AN-MA membranes varied with AN-MA concentration and feed ratio of MA. The membranes were prepared from the ternary system with 75 wt.% EC content in the mixed diluent.

membranes. Therefore, the water flux and porosity of the P2 membranes are excellent when the MA content is 20 mol%.

### 3.4.2. Effects of EC and MA content on the water flux and porosity of the membrane

The water flux and porosity of the AN-MA membranes prepared from different mixed diluent systems at 9 and 15 wt.% AN-MA concentrations are shown in Figs. 13 and 14. The results indicate that the water flux and porosity of the AN-MA membranes are strongly affected by the ratio of the mixed diluent. The porosity

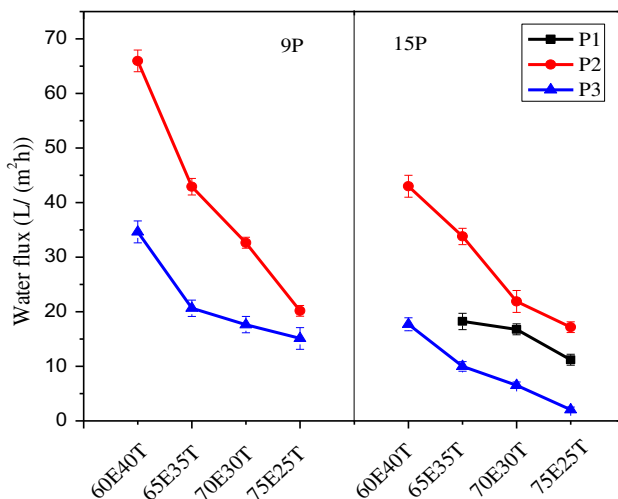


Fig. 13. Water flux of AN-MA membranes as a function of EC and MA contents. The membranes were prepared from the ternary system with 9 and 15 wt.% AN-MA concentrations.

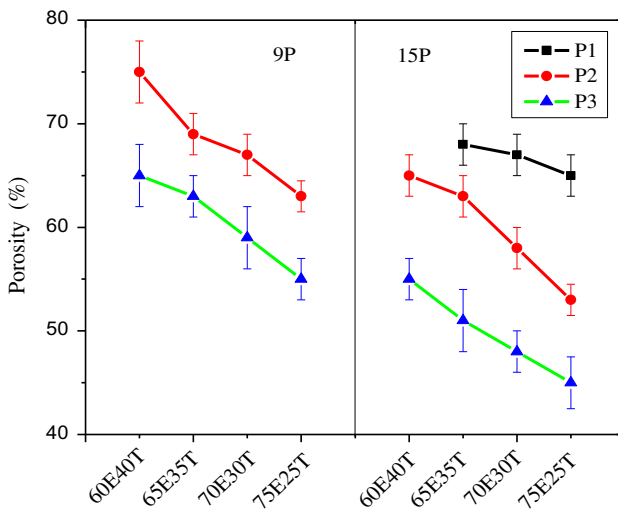


Fig. 14. Porosity of AN-MA membranes as a function of EC and MA contents. The membranes were prepared from the ternary system with 9 and 15 wt.% AN-MA concentrations.

and water flux of the microporous membranes increase with decreasing EC content in the mixed diluent. EC is a good solvent for PAN; the compatibility between the polymer and mixed diluent improves with increasing EC content, resulting in a lower cloud point of the ternary system. Therefore, the cellular structure resulting from the droplet growth is rapidly locked in upon quenching the sample due to the rapid heat transfer, resulting in the decrease in the porosity and water flux of the AN-MA membranes with

increasing EC content in the mixed diluent. The bulk microstructure of the flat membrane prepared by the diluent mixture with 60E40T and 65E35T exhibits an interconnected sponge-like microstructure due to the system proceeding via spinodal decomposition of L–L phase separation. Thus, AN-MA membranes fabricated from 9P2 (60E40T) and 9P2 (65E35T) exhibit a higher water flux and porosity.

### 3.5. Mechanical properties

Tensile tests were performed to investigate the mechanical properties of the AN-MA membranes. The mechanical properties of the AN-MA microporous membranes prepared with various MA and EC contents in the mixed diluent are shown in Figs. 15 and 16. The tensile strength and elongation of the AN-MA membranes increase with increasing AN-MA concentration and EC content, which is caused by the decrease of the membrane porosity [41]. The cross-section structure of the AN-MA membranes changes from interconnected network pores to cellular pores with the emergence of closed pores with increasing EC content. This finding indicates that the uniform sponge-like microstructure formed via L–L phase separation for the AN-MA membrane is the dominant factor responsible for its mechanical strength. An explanation for the change in the break elongation might be that the decrease in porosity is favorable to the increase in break elongation [42,43]. It is

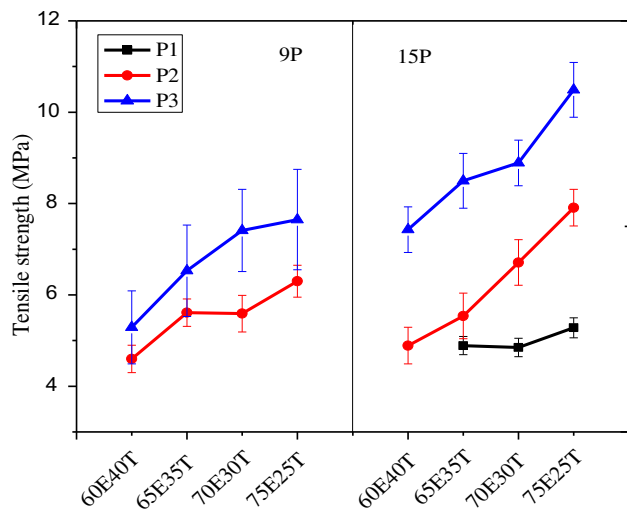


Fig. 15. Tensile strength of AN-MA membranes varied with AN-MA concentration and MA and EC contents. The membranes were prepared from the ternary system with 9 and 15 wt.% AN-MA concentrations.

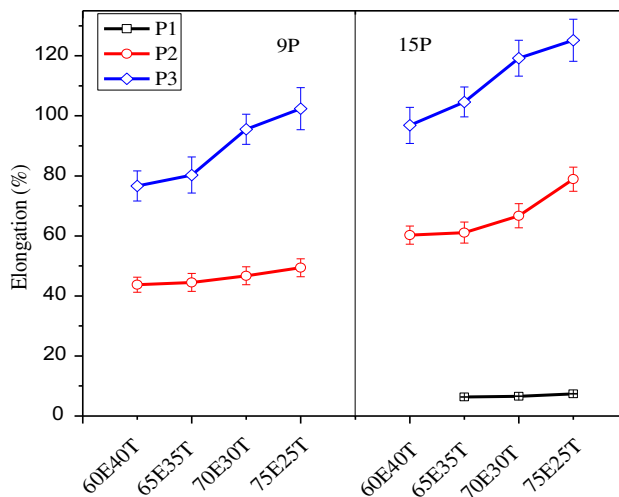


Fig. 16. Elongation of AN-MA membranes varied with AN-MA concentration and MA and EC contents. The membranes were prepared from the ternary system with 9 and 15 wt.% AN-MA concentrations.

commonly believed that an interconnected network structure with higher porosity usually exhibits poorer mechanical properties than a cellular-like structure. Thus, the lower porosity of the AN-MA membrane is beneficial for the mechanical properties of AN-MA membranes. Increasing the AN-MA concentration makes the mutual entanglement between macromolecules closer, resulting in the increasing of the tensile strength and elongation of AN-MA membranes. In addition, for the solution with higher AN-MA concentration, the elevation of the system viscosity suppresses the nucleation and growth of the diluent-rich phase, and the pore size and porosity of the resulting membranes are relatively small. Consequently, the mechanical properties of AN-MA microporous membranes increase with increasing polymer concentration.

The P2 and P3 membranes are also observed to possess higher tensile strength and elongation at break relative to the P1 membrane. On the one hand, MA is used as a flexible second monomer to copolymerize with acrylonitrile (AN) to weaken the force between the dipoles and reduce the sequence length of the cyano unit on the PAN macromolecular chain. On the other hand, the molecular weight of AN-MA increases with increasing MA content from 15 to 25 mol%. The increasing of the casting solution viscosity is not conducive to the spread and aggregation of diluent, yielding smaller pores and lower porosity. The decrease in the porosity is favorable to the increase in break elongation. The tensile strength and elongation

at break of the P1 membrane prepared from 15P1 (75E25T) are 5.5 MPa and 3.2%, respectively, whereas the membranes prepared from 15P2 (75E25T) and 15P3 (75E25T) exhibit higher tensile strength (7.9 and 10.5 MPa) and elongation (79.0 and 125.0%), respectively.

#### 4. Conclusions

Poly(acrylonitrile-methacrylate) (AN-MA) membranes have been successfully prepared via the TIPS process using ethylene carbonate (EC)/triethyl citrate (TEC) as the mixed diluent. The effects of the preparation conditions, such as the MA feeding mole ratio, EC content in the mixed diluent, and AN-MA concentration, on the pore structure, porosity, water flux, and mechanical properties of the AN-MA membranes were investigated. The results indicate that both the mixed diluent ratio and AN-MA concentration can affect the phase diagram during the TIPS process, which ultimately affects the phase separation mechanism. A lower EC content and lower AN-MA concentration are more likely to lead to phase separation occurring according to spinodal phase splitting, which results in an interconnected dendritic or network structure. Conversely, if the phase separation mechanism is the nucleation-growth mechanism, the structure of the cross section will be an open/closed cellular-like structure. With increasing MA feeding molar ratio in the polymerization system, the water flux of AN-MA membranes increases and then decreasing, and the mechanical properties of the AN-MA membranes increase gradually. The membranes prepared from 15P2 (75E25T) and 15P3 (75E25T) exhibit higher tensile strength (7.9 and 10.5 MPa, respectively) and elongation (79.0 and 125.0%, respectively). Consequently, the properties of AN-MA membranes are optimal when the MA feeding molar ratio is 20 mol %. The membrane fabricated from 9P2 (60E40T) exhibits the highest water flux (66.0 L/(m<sup>2</sup> h)) and a higher tensile strength (4.6 MPa) and elongation (43.8%).

#### Acknowledgments

The authors are thankful to the National Natural Science Foundation of China (21206123); Doctoral Program of Higher Education of China (20111201120001); China Postdoctoral Science Foundation (2014M551026), Postdoctoral Foundation of Shan Dong Province (201402011); Natural Science Foundation of Tianjin City (13JQCQNJC02300) for financial support.

#### A list of symbols

$M_n$	—	number average molecular weight
$M_w$	—	weight average molecular weight
$T_m$	—	melting temperature
$T_d$	—	decomposition temperature
$J_w$	—	water flux
$V$	—	volume of permeated water
$A$	—	membrane area
$\Delta t$	—	permeation time
$\varepsilon$	—	porosity of the wet AN-MA membrane
$m_1$	—	weight of the wet AN-MA membrane
$m_2$	—	weight of the dry AN-MA membrane
$\rho_{\text{water}}$	—	density of water
$\rho_{\text{AN-MA}}$	—	density of AN-MA copolymer
$\delta$	—	solubility parameter
$\delta_d$	—	dispersion parameter
$\delta_p$	—	polar parameter
$\delta_h$	—	hydrogen bonding parameter
$i$	—	number of structural groups
$F_{d,i}; F_{p,i}$	—	group molar attractions
$E_{h,i}$	—	cohesive energy contributed from hydrogen bonding.

#### References

- [1] J. Yang, D.W. Li, Y.K. Lin, X.L. Wang, F. Tian, Z. Wang, Formation of a bicontinuous structure membrane of polyvinylidene fluoride in diphenyl ketone diluent via thermally induced phase separation, *J. Appl. Polym. Sci.* 110 (2008) 341–347.
- [2] X. Li, X. Lu, Morphology of polyvinylidene fluoride and its blend in thermally induced phase separation process, *J. Appl. Polym. Sci.* 101 (2006) 2944–2952.
- [3] S. Song, J.M. Torkelson, Coarsening effects on the formation of microporous membranes produced via thermally induced phase separation of polystyrene-cyclohexanol solutions, *J. Membr. Sci.* 98 (1995) 209–222.
- [4] H. Matsuyama, H. Okafuji, T. Maki, M. Teramoto, N. Kubota, Preparation of polyethylene hollow fiber membrane via thermally induced phase separation, *J. Membr. Sci.* 223 (2003) 119–126.
- [5] S.S. Kim, D.R. Lloyd, Microporous membrane formation via thermally induced phase separation. III. Effect of thermodynamic interactions on the structure of isotactic polypropylene membranes, *J. Membr. Sci.* 64 (1991) 13–29.
- [6] D.R. Lloyd, S.S. Kim, K.E. Kinzer, Microporous membrane formation via thermally-induced phase separation. II. Liquid-liquid phase separation, *J. Membr. Sci.* 64 (1991) 1–11.
- [7] M.H. Gu, J. Zhang, X.L. Wang, Crystallization behavior of PVDF in PVDF-DMP system via thermally induced phase separation, *J. Appl. Polym. Sci.* 102 (2006) 3714–3719.
- [8] Z.Y. Cui, C.H. Du, Y.Y. Xu, G.L. Ji, B.K. Zhu, Preparation of porous PVDF membrane via thermally induced phase separation using sulfolane, *J. Appl. Polym. Sci.* 108 (2007) 272–280.

- [9] Y.K. Lin, Y.H. Tang, H.Y. Ma, J.Y. Yang, Y. Tian, W. Ma, Formation of a bicontinuous structure membrane of polyvinylidene fluoride in diphenyl carbonate diluent via thermally induced phase separation, *J. Appl. Polym. Sci.* 114 (2009) 1523–1528.
- [10] H. Matsuyama, T. Maki, M. Teramoto, K. Asano, Effect of polypropylene molecular weight on porous membrane formation by thermally induced phase separation, *J. Membr. Sci.* 204 (2002) 323–328.
- [11] M.C. Yang, J.S. Perng, Microporous polypropylene tubular membranes via thermally induced phase separation using a novel solvent-camphene, *J. Membr. Sci.* 187 (2001) 13–22.
- [12] M.H. Gu, J. Zhang, X.L. Wang, H.J. Tao, L.T. Ge, Formation of poly(vinylidene fluoride) (PVDF) membranes via thermally induced phase separation, *Desalination* 192 (2006) 160–167.
- [13] Z.S. Yang, P.L. Li, L.X. Xie, Z. Wang, S.C. Wang, Preparation of iPP hollow-fiber microporous membranes via thermally induced phase separation with co-solvents of DBP and DOP, *Desalination* 192 (2006) 168–181.
- [14] H. Matsuyama, M. Teramoto, S. Kudari, Y. Kitamura, Effect of diluents on membrane formation via thermally induced phase separation, *J. Appl. Polym. Sci.* 82 (2001) 169–177.
- [15] B.J. Cha, K. Char, J.J. Kim, S.S. Kim, C.K. Kim, The effects of diluent molecular weight on the structure of thermally-induced phase separation membrane, *J. Membr. Sci.* 108 (1995) 219–229.
- [16] K. Yoon, B.S. Hsiao, B. Chu, High flux ultrafiltration nanofibrous membranes based on polyacrylonitrile electrospun scaffolds and crosslinked polyvinyl alcohol coating, *J. Membr. Sci.* 338 (2009) 145–152.
- [17] R. Saranya, G. Arthanareeswaran, S. Sakthivelu, P. Manohar, Preparation and performance evaluation of nanokaolinite-particle-based polyacrylonitrile mixed-matrix membranes, *Ind. Eng. Chem. Res.* 51 (2012) 4942–4951.
- [18] B. Jung, J.K. Yoon, B. Kim, H.W. Rhee, Effect of molecular weight of polymeric additives on formation, permeation properties and hypochlorite treatment of asymmetric polyacrylonitrile membranes, *J. Membr. Sci.* 243 (2004) 45–57.
- [19] A. Désormeaux, M.E. Moreau, Y. Lepage, J. Chanard, A. Adam, The effect of electronegativity and angiotensin-converting enzyme inhibition on the kinin-forming capacity of polyacrylonitrile dialysis membranes, *Biomaterials* 29 (2008) 1139–1146.
- [20] Z.G. Wang, L.S. Wan, Z.K. Xu, Surface engineering of polyacrylonitrile-based asymmetric membranes towards biomedical applications: An overview, *J. Membr. Sci.* 304 (2007) 8–23.
- [21] J. Ma, M.H. Zhang, H. Wu, X. Yin, J. Chen, Z.Y. Jiang, Mussel-inspired fabrication of structurally stable chitosan/polyacrylonitrile composite membrane for pervaporation dehydration, *J. Membr. Sci.* 348 (2010) 150–159.
- [22] H.A. Tsai, Y.L. Ye, K.R. Lee, S.H. Huang, M.C. Suen, J.Y. Lai, Characterization and pervaporation dehydration of heat-treatment PAN hollow fiber membranes, *J. Membr. Sci.* 368 (2011) 254–263.
- [23] H.A. Tsai, W.H. Chen, C.Y. Kuo, K.R. Lee, J.Y. Lai, Study on the pervaporation performance and long-term stability of aqueous iso-propanol solution through chitosan/polyacrylonitrile hollow fiber membrane, *J. Membr. Sci.* 309 (2008) 146–155.
- [24] Q.Y. Wu, L.S. Wan, Z.K. Xu, Structure and performance of polyacrylonitrile membranes prepared via thermally induced phase separation, *J. Membr. Sci.* 409–410 (2012) 355–364.
- [25] H.Q. Liang, Q.Y. Wu, L.S. Wan, X.J. Huang, Z.K. Xu, Polar polymer membranes via thermally induced phase separation using a universal crystallizable diluent, *J. Membr. Sci.* 446 (2013) 482–491.
- [26] Q.Y. Wu, B.T. Liu, M. Li, L.S. Wan, Z.K. Xu, Polyacrylonitrile membranes via thermally induced phase separation: Effects of polyethylene glycol with different molecular weights, *J. Membr. Sci.* 437 (2013) 227–236.
- [27] N. Han, X.X. Zhang, W.Y. Yu, X.Y. Gao, Effects of copolymerization temperatures on structure and properties of melt-spinnable acrylonitrile-methyl acrylate copolymers and fibers, *Macromol. Res.* 18 (2010) 1060–1069.
- [28] J. Brandrup, E.H. Immergut, E.A. Grulke, *Polymer Handbook*, Wiley, New York, NY, 1999.
- [29] V.A. Bhanu, P. Rangarajan, K. Wiles, M. Bortner, M. Sankarpandian, D. Godshall, T.E. Glass, A.K. Banthia, J. Yang, G. Wilkes, Synthesis and characterization of acrylonitrile methyl acrylate statistical copolymers as melt processable carbon fiber precursors, *Polymer* 43 (2002) 4841–4850.
- [30] N. Han, X.Y. Gao, R. Zhang, X.X. Zhang, Structures and properties of thermoregulated acrylonitrile-methyl acrylate sheet containing microphase change materials, *Polym. Compos.* 34 (2013) 641–649.
- [31] X.Y. Gao, N. Han, X.X. Zhang, W.Y. Yu, Melt-processable acrylonitrile-methyl acrylate copolymers and melt-spun fibers containing MicroPCMs, *J. Mater. Sci.* 44 (2009) 5877–5884.
- [32] C.V. Funk, B.L. Beavers, D.R. Lloyd, Effect of particulate filler on cell size in membranes formed via liquid-liquid thermally induced phase separation, *J. Membr. Sci.* 325 (2008) 1–5.
- [33] X.F. Li, Y.G. Wang, X.L. Lu, C.F. Xiao, Morphology changes of polyvinylidene fluoride membrane under different phase separation mechanisms, *J. Membr. Sci.* 320 (2008) 477–482.
- [34] D.W. Van Krevelen, K. Te Nijenhuis, *Properties of Polymers (fourth ed.)*, Chapter 7—Cohesive Properties and Solubility, Elsevier, Netherlands, 2009, pp. 189–227.
- [35] B.D. Coleman, Application of the theory of absolute reaction rates to the creep failure of polymeric filaments, *J. Polym. Sci.* 20 (1956) 447–455.
- [36] H. Matsuyama, Y. Takida, T. Maki, M. Teramoto, Preparation of porous membrane by combined use of thermally induced phase separation and immersion precipitation, *Polymer* 43 (2002) 5243–5248.
- [37] H. Komiyama, *Rate Processes*, Asakura Syoten, Tokyo, 1990 (in Japanese).
- [38] P.L. Hanks, D.R. Lloyd, Deterministic model for matrix solidification in liquid-liquid thermally induced phase separation, *J. Membr. Sci.* 306 (2007) 125–133.

- [39] S.P. Nunes, T. Inoue, Evidence for spinodal decomposition and nucleation and growth mechanisms during membrane formation, *J. Membr. Sci.* 111 (1996) 93–103.
- [40] X. Fu, H. Matsuyama, M. Teramoto, H. Nagai, Preparation of hydrophilic poly(vinyl butyral) hollow fiber membrane via thermally induced phase separation, *Sep. Purif. Technol.* 45 (2005) 200–207.
- [41] H. Zhang, Y.L. Zhao, H.T. Wang, W. Zhong, Q.G. Du, X.M. Zhu, Phase behavior of polyetherimide/benzophenone/triethylene glycol ternary system and its application for the preparation of microporous membranes, *J. Membr. Sci.* 354 (2010) 101–107.
- [42] V. Jousseume, G. Rolland, D. Babonneau, J.P. Simon, Influence of polymer porogens on the porosity and mechanical properties of spin coated ultra low  $k$  dielectrics, *Thin Solid Films* 517 (2009) 4413–4418.
- [43] M. Ahmed, H. Ghanbari, B.G. Cousins, G. Hamilton, A.M. Seifalian, Small calibre polyhedral oligomeric silsesquioxane nanocomposite cardiovascular grafts: Influence of porosity on the structure, haemocompatibility and mechanical properties, *Acta Biomater.* 7 (2011) 3857–3867.